Master of Physics

Orbital Hall magnetoresistance of epitaxially grown Fe/Cr bilayers

Department of Physics and Laboratory for Spin-Orbitronic Devices,

University of Ulsan, Ulsan 44610, Republic of Korea

Vu Minh Thanh

Orbital Hall magnetoresistance of epitaxially grown Fe/Cr bilayers

Supervisor: Sanghoon Kim

A Dissertation submitted to the Graduate School of the University of Ulsan in partial Fulfillment of the requirements for the Degree of
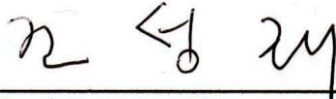
Master of Physics

April 2023

by

Vu Minh Thanh

Department of Physics and Laboratory for Spin-Orbitronic Devices,

University of Ulsan, Ulsan 44610, Republic of Korea

Orbital Hall magnetoresistance of epitaxially grown Fe/Cr bilayers

This is to declare that the dissertation

submitted by Vu Minh Thanh is approved officially.

Committee Chair: Prof. Sunglae Cho

Department of Physics, University of Ulsan

Committee Member: Prof. Sonny Rhim

Department of Physics, University of Ulsan

Committee Member and Supervisor: Prof. Sanghoon Kim

Department of Physics, University of Ulsan

Department of Physics and Laboratory for Spin-Orbitronic Devices,

University of Ulsan, Ulsan 44610, Republic of Korea

June 2023

Acknowledgements

I would like to express my sincere gratitude to my thesis advisor Professor Sanghoon Kim, for his invaluable guidance, patience, and unwavering support throughout the research process. His expertise, constructive feedback, and commitment to excellence have been instrumental in shaping this thesis.

I am also grateful to the faculty members in the Department of Physics for their valuable insights, comments, and suggestions that have helped me to improve the quality of my work. Their teachings, encouragement, and mentorship have been a great source of inspiration for me.

I would like to thank my colleagues and friends for their encouragement, motivation, and assistance during this journey. Their invaluable contributions, both academically and personally, have made this thesis possible.

I am deeply grateful to my family for their unconditional love, support, and encouragement. Their unwavering belief in me has been a constant source of strength and inspiration.

Finally, I would like to express my heartfelt appreciation to all those who have contributed to this thesis in one way or another. Your support, encouragement, and guidance have been instrumental in making this thesis a reality. Thank you.

Abstract

During the last two decades, spin Hall effect has been intensively studied, because pure spin current can be generated in a non-ferromagnetic metal with strong spin orbit coupling, e.g., Pt, W or Ta. By the way, in recent few years, it has been demonstrated that orbital Hall effect occurs in light metal systems such as Cr. In this study, orbital dependent magnetoresistance, namely orbital Hall magnetoresistance (OMR), is observed in epitaxially grown Fe/Cr bilayers to see how the crystal texture can affect the orbital transport phenomena. The SMR signal showed similarity trend in both current direction I[100] and I[110] and the maximum value SMR ~ 0.7 is comparable with other systems with the same characteristics. We also propose a reliable method to fit the SMR signal when the external magnetic field is under saturate field of sample, the advantage and disadvantage of this method will also be discussed.

Outline

List of figures

Fig 14. Device shape and the current set up

Fig 15. Sample composition and current direction I[100] and I[110], the blue part is the substrate MgO

Fig 16. Sample structure and image device for I[110] and I[100] set of Fe/Cr(2nm)

Fig 17. Angular dependent of OMR under external field 21k Oe in the yz plane

Fig 18. The relation between θ_M and θ_H

Fig 19. Converting values from θ_H to θ_M

Fig 20. Thickness dependence of OMR

List of Equations

Eq 1. Spin Hall angle definition

Eq 2. Spin orbit coupling energy

Eq 3. OMR equation

Eq 4. Bragg law

Eq 5. Thickness measurement

Eq 6. OMR theory

Eq 7. the energy E of its magnetic moment under the external magnetic field H

Eq 8. The relation between θ_M and θ_H

1. Introduction

In recent years, spintronics has emerged as a promising field for developing novel electronic devices with improved functionality and performance. One of the key concepts in spintronics is the manipulation of the spin degree of freedom in addition to the traditional charge degree of freedom. Spin Hall Magnetoresistance (SMR) is a phenomenon that arises from the interplay between spin and charge transport in a heavy metal (HM) layer adjacent to a ferromagnetic (FM) layer [1]. The SMR effect leads to a change in the resistance of the sample, and has been the subject of intense research in the past decade due to its potential for various applications such as magnetic sensors, non-volatile memory, and logic devices [2].

The SMR effect originates from the Spin Hall effect, which was first predicted by Dyakonov and Perel in 1971, and experimentally observed in heavy metals by Hirsch in 1999 [3, 4]. The Spin Hall effect is a relativistic effect that arises from the spin-orbit coupling in a non-magnetic material, and leads to the generation of a spin current transverse to an applied charge current. In the context of SMR, the spin current generated in the HM layer diffuses into the adjacent FM layer and exerts a torque on the magnetization of the FM, leading to a change in its resistance. The magnitude and sign of SMR can depend on various factors, such as the thickness, conductivity, and spin-orbit coupling strength of the HM layer, the interface quality between the FM and HM layers, and the direction and magnitude of the applied current.

Moreover, recent theory reports a similar phenomenon called Orbital Hall Effect (OHE) which induces a flow of orbital, in other words, a current of orbital angular momentum [5 - 8]. Unlike the SHE which often requires material with strong spin orbit coupling, the OHE theory bases on the momentum space orbital textures which generally occurs in a number of systems, even in

system that does not have strong spin orbit coupling [7]. Another reason why OHE gains much interested recently is that theoretical calculations predict that in some systems commonly popular for spin orbit torque such as Ta and W [5, 6, 8], Orbital Hall conductivity is found to be much larger than Spin Hall conductivity. This indicates the OHE can be the current origin of spin orbit torque and magnetoresistance observed in some system where SHE is relatively ignored [9]. Yet the mechanism of OHE is still under investigation, one should be noted that the orbital current can only interact with the magnetization indirectly through spin angular momentum, in other words, the orbital is expected to be converted into spin then transfer the angular momentum to magnetization. That is to say, the mechanism of OHE and SHE is somehow a combination and can be studied both together.

In this work, we focus on the thickness dependence of Orbital Hall Magnetoresistance (OMR) in a bilayer Fe/Cr structure. Fe is chosen due to its strong ferromagnetic, Cr is chosen as an orbital current source material because theoretically Cr has large orbital Hall conductivity ~ $8200(\hbar/e)(\Omega\,cm)^{-1}$ while the spin Hall conductivity is insignificant ~ $130(\hbar/e)(\Omega\,cm)^{-1}$ [8]. We fabricate two sets of samples with different current directions, I[110] and I[100] with intention of observing different orbital texture, and investigate the OMR as a function of Cr thickness in the range of 2-20 nm. By systematically varying the thickness of the Cr layer, we can explore the effect of orbital diffusion length, interface scattering, and other mechanisms on OMR. Our experimental setup allows us to measure the resistance of the FM layer as a function of the applied current direction and voltage, and extract the OMR ratio. We also use theory to predict the trend of experiment OMR data. From the fitting results, important parameters of sample such as orbital diffusion length, orbital mixing conductance and orbital Hall angle have been revealed.

The purpose of this paper is to provide a comprehensive study of the thickness dependence of OMR in bilayer Fe/Cr, and to shed light on the underlying mechanisms and characteristics of this effect. We hope that our results can contribute to the further optimization and development of OMR-based spintronic devices with enhanced performance and functionality.

2. Theoretical background

Spintronics is a research field which utilizes spin degree of freedom of the electron for high speed, low power consumption electronic devices. During last two decades, spin Hall effect has been intensively studied, because pure spin current can be generated in a non-ferromagnetic metal with strong spin orbit coupling, e.g., Pt, W or Ta. By the way, in recent few years, orbital Hall effect occurs in light metal systems such as Cr. In this study, orbital dependent magnetoresistance, namely orbital Hall magnetoresistance (OMR), is observed in epitaxially grown Fe/Cr bilayers to see how the crystal texture can affect the orbital transport phenomena.

2.1 Spin Hall effect (SHE) and Inverse Spin Hall effect (ISHE)

From not long ago, a new spintronics realm was discovered and opening new aspect of studying electric current. That is to say, the current is not only has charge property but also the spintronics one [10, 11]. Unlike the ongoing debate - extended phenomenon and applications such as the anisotropic magnetoresistance (AMR) which refers to relationship of the resistance of ferromagnet and the angle between the current and magnetization direction [12 - 14], or similar
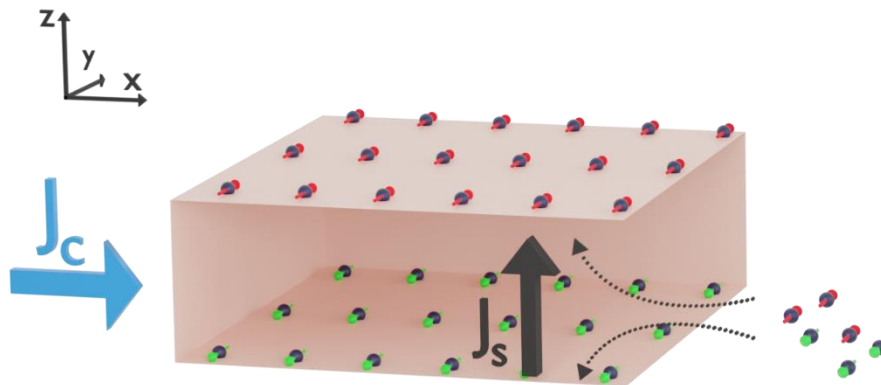
Fig 1. Spin current induced in lateral surfaces of material by charge current (SHE)

effects of the giant magnetoresistance (GMR) and tunneling magnetoresistance (TMR), the origin

of spintronics would be rather simple and focus on Spin Hall effect (SHE) and Inverse Spin Hall effect (ISHE).

The Spin Hall effect (SHE) is a transport phenomenon found by Russian physicists Mikhail I. Dyakonov and Vladimir I. Perel in 1971 [3, 4] which predicts the spin accumulation induced on the lateral surfaces of material with charge current flowing through [Fig 1]. The electrons J_C with different spins (up and down) travel to opposite side on the surface of material and result in a flow of current J_S which is perpendicular to the original charge current. The Inverse Spin Hall effect (ISHE) is rather similar to SHE mechanism, in the inverse way, in other words, the spin current plays role as a source to produce charge current [Fig 2]. The physical origin of this effect – aka SHE – is believed to be caused by either extrinsic or intrinsic properties of material. Both of them refer to the interaction between spins in charge current and atoms in material which results in spin accumulation at opposite sides depending on different spin direction. The extrinsic theory proposed by Dyakonov and Perel suggests that when the charge current moves inside material, its electrons collide with impurities in the material and diffuse into different directions. More specifically, the intrinsic mechanism implies on the asymmetries in the material which applies spin orbit interaction on carriers and modifies their trajectories.

One of the most important in SHE is how efficiency this process is or in other words, how much of the charge current can be transferred into spin current. The Spin Hall angle θ_{SH}, which shares similar concept as original Hall effect, is introduced to measure that quantity:

$$\theta_{SH} = \frac{J_S}{J_C} \quad \textbf{[Eq 1]}$$

Whereas J_S is the spin current as an output, J_C is the charge current as a source.

2.2 Spin orbit coupling
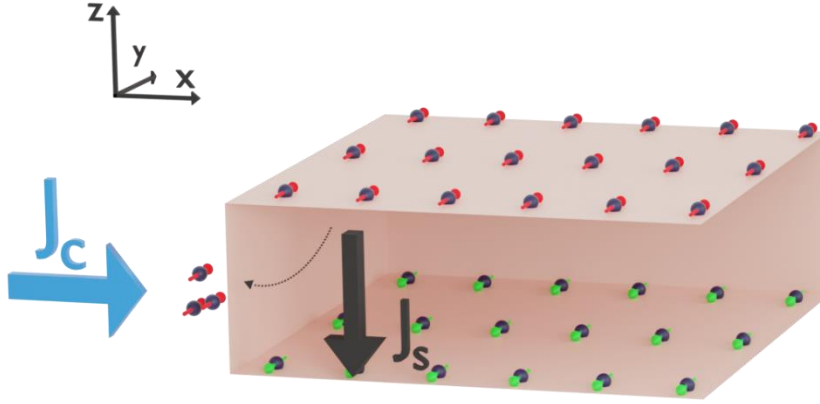
Fig 2. Mechanism of Inverse Spin Hall effect (ISHE)

Spin orbit coupling is the interaction between the electron's spin and its motion trajectory around the nuclear. Originate from the Quantum mechanics, the electron moves with eclipse trajectory around nuclear at center, this motion induces a well-known relativistic effect $\vec{L}$ (orbital spin), in the meantime, the electron also rotates itself and creates another electromagnetic field $\vec{S}$ (intrinsic spin) **[Fig 3]**. The two of them interact with each other leading to a shift in the electron's atomic energy levels called total angular momentum. Their energy can be presented as:

$$H_{SOC} = -\frac{e\hbar}{4m^2c^2}\boldsymbol{\sigma}\cdot[\boldsymbol{E}\times\boldsymbol{p}] \quad \textbf{[Eq 2]}$$
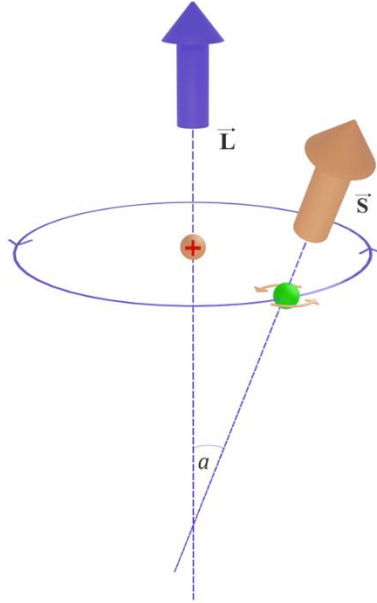
Fig 3. Spin orbit/HM system coupling mechanism

2.3 Magnetoresistance (MR)

The magnetoresistance (MR) is a varying resistance phenomenon of material while applying an external magnetic field. There is a numerous effect that can be origin of MR which is depending on the type of material. In term of shape, bulk non-magnetic metal and semiconductors, which have MR value depended strongly on the mobility and external magnetic field, have MR derived from geometrical magnetoresistance **[15]**. Unlike bulk material, multilayer system has their resistance properties depends not only on the material, but also the interface interaction. A typical bilayer would have a normal metal/non-magnetic metal (NM) which is a source for charge current and a ferromagnet material (FM) which affects the resistance based on how their magnetization orients. In such a system, the origin of MR is normally explained and observed by anisotropy magnetoresistance (AMR) in which changing angle between the current direction and

magnetization of FM layer directly affects the resistance of material **[12 - 14]**; giant magnetoresistance (GMR) **[16]** and tunneling magnetoresistance (TMR) **[17, 18]** which are found regularly in magnetic field sensors and data storage devices application.

2.4 Orbital Hall magnetoresistance (OMR) in FM/HM bilayer structure

Due to its potential use in spintronic and magnetoelectronic devices, orbital Hall magnetoresistance (OMR), a fascinating phenomenon, has attracted a lot of attention lately **[19]**. OMR is seen in bilayer structures made of ferromagnets and normal metals (FM/HM), where resistance changes happen in response to an applied magnetic field that is perpendicular to the current flow. The interaction of the spin and orbital degrees of freedom in the system, specifically through the spin-orbit coupling (SOC) phenomenon brought on by the ferromagnetic layer, is thought to represent the underlying mechanism of OMR **[20 - 25]**. The origin of Orbital Hall magnetoresistance is believed to be from Orbital Hall effect (OHE), instead of a flow of spin current like SHE, a flow of orbital current is detected in the case of OHE. That current shares similar mechanism like SHE, the angular momentum L is defined from localized orbitals around the atom at each lattice. With the help of the spin-orbit torque (SOT), which is created by the SOC, electrons in the nearby normal metal layer can transfer angular momentum from their spin to their orbital motion. The Hall current, which is a transverse charge current produced by this SOT-induced orbital motion, runs perpendicular to both the applied magnetic field and the current's direction. By enabling new features and better performance in electronic devices, the OMR effect, which appears as changes in resistance along the transverse direction, has the potential to completely transform spin-based technology. Explosive possibilities for utilizing spin and orbital degrees of freedom for next-generation spintronic and magnetoelectronic applications have

emerged from the research of OMR in FM/HM bilayer structures. It is believed that more research in this area would enable spin-based technologies to evolve at a cutting-edge rate and unleash the full potential of OMR.

To study the OMR phenomenon, first one should be able to achieve the SMR mechanism. In FM/HM bilayer systems, spin Hall magnetoresistance (SMR), a novel magnetoresistance, has also been found [26]. The original of this magnetoresistance originates from the charge current scattering caused by the SHE in the HM layer. The charge current J_C flowing in the HM layer partly experiences spin-dependent scattering, causing the flow of the pure spin current J_S orthogonal to the charge current direction [27]. One important thing is that the spin polarization σ is orthogonal to both charge current J_C and spin current J_S [Fig 1]. A part of J_S (red ones) is going to enter the FM layer and the way it interacts with the magnetization of FM layer depends on the
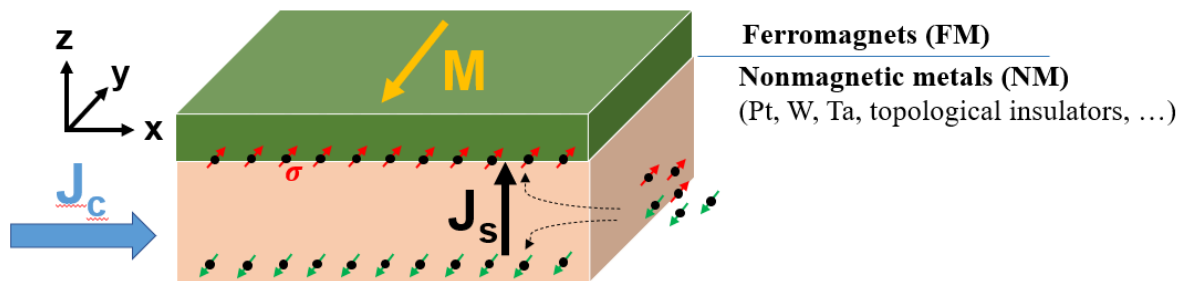
Fig 4. SHE in FM/HM system

direction of **M** and σ when **M** is the magnetization of FM layer [Fig 4].

Then we have two cases of low resistance and high resistance in this kind of system.

Case 1: the low resistance case [Fig 5a], the magnetization **M** is collinear to spin polarization σ, the spin current entering the FM is conserved and accumulated therein since the energy exchange of spin transfer torque is minimum [28]. Through the inverse SHE mechanism, this spin

accumulation in turn creates a reverse flow toward the HM and forms a charge current in the HM. As a result, the overall loss of the charge current is minimal, which causes the FM/HM bilayer to have a high conductivity, in other words, the resistance is low in this case.

Case 2: the high resistance case **[Fig 5b]**, the magnetization **M** is perpendicular to spin polarization $\boldsymbol{\sigma}$, because of the spin transfer torque, the magnetization dissipates the spin current **[28]**, which reduces the spin current's ability to flow backward and induce the charge current. Low conductivity is actually caused by the loss of the charge current in the FM/HM bilayer. This case introduces high resistance than the previous one.

From both cases, we can observe that the resistance change due to SMR depends on the angle between magnetization **M** of FM layer and spin polarization $\boldsymbol{\sigma}$. Follow that, an experiment is set up to change the angle between them (external field rotates in yz plane) **[Fig 5c]**, and we can calculate the SMR with the follow equation:

$$SMR = \frac{R_{xx} - R_0}{R_0} \qquad \textbf{[Eq 3]}$$

Whereas R_{xx} is the resistance measured at various selected time, R_0 is the maximum resistance which is recorded when **M** is perpendicular to $\boldsymbol{\sigma}$.
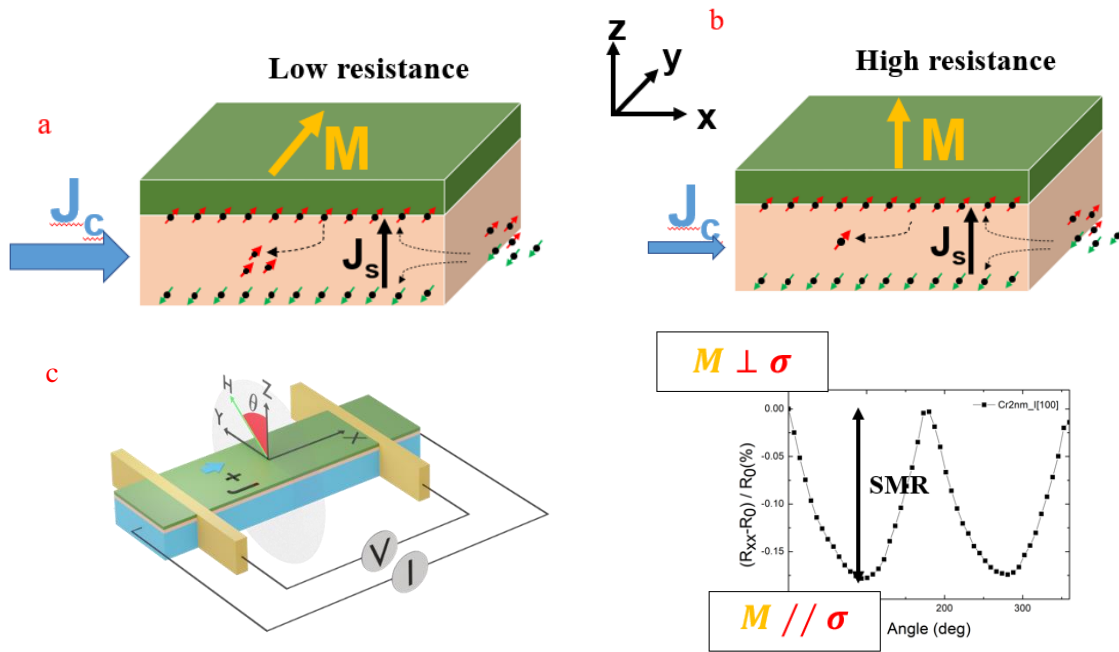
Fig 5. Mechanism of SMR with a) low resistance,
b) high resistance and c) set up the angle rotation

The OMR also comes with two case of high resistance and low resistance. If the magnetization of FM is perpendicular to the orbital angular momentum (OAM), the OAM is absorbed by the FM as it exerts a torque on the magnetization (high resistance). When the magnetization direction is parallel to the direction of the OAM (low resistance), the OAM is reflected from the interface. It should be noted that, the OMR and SMR are quite similar which makes it difficult to distinguish between them. One important point is while the SMR required material with strong spin orbit coupling, the OMR does not. When an electrical field is applied, the energy can be transferred to localized orbital of atom, the second stage is interaction between orbital and spin through spin orbit coupling. So, the OMR will always occur even with material with insignificant spin orbit coupling and then maybe used to explain the magnetoresistance phenomenon better than SMR theory.

With that in mind, we choose Chromium as NM layer to study the OMR since Cr has a significant high value of orbital Hall conductivity **[8]** $\sigma_{OH} = 8200 \ (\hbar/e)(\Omega \cdot cm)^{-1}$ while the spin Hall conductivity is neglectable $\sigma_{SH} = -130 \ (\hbar/e)(\Omega \cdot cm)^{-1}$. We also choose to fabricate two set of current direction (on substrate) I[110] and I[100] which should gives different orbital texture behavior. The Fe is chosen as FM layer since it is very popular among FM material.

3. Experimental method

This chapter presents all the experimental methods used in this work. First, to fabricate the samples, photolithography and ion milling are introduced as reliable and popular options. Then, X-Ray diffraction and X-Ray reflectivity are presented to examine the sample's structure and quality. Finally, R_{xx} measurement will be carried out to study about the magnetic properties of thin films material.

3.1 Mask design

To study the Orbital Hall magnetoresistance (OMR) at interface of bilayer Fe/Cr, the device structure must be designed in detail at nanometer scale. Here at the laboratory, we first made the
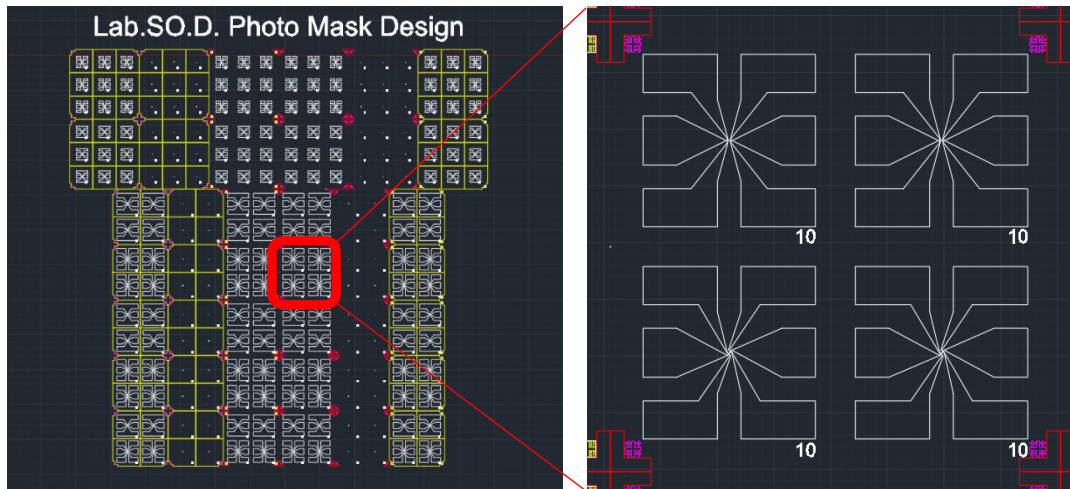
Fig 6. Mask design of sample in CAD format

basic 4 points contact scheme in CAD program. This design **[Fig 6]** is flexible for studying most popular spintronics phenomenon such as Anisotropy magnetoresistance, Spin Hall magnetoresistance, and Anomalous Hall effect

3.2 Photolithography

When it comes to structuring and patterning materials at the micro and nanoscale, photolithography is a crucial nanofabrication technology that is utilized extensively in science and engineering. It involves using light to a substrate coated with a photosensitive substance, usually a photoresist, to transfer a pattern from a mask onto the substrate. Photolithography enables for the exact and repeatable creation of complex structures with feature sizes ranging from sub-micrometer to nanoscale scale through a sequence of well-controlled stages, including exposure, development, and etching. This method has found use in a variety of industries, including microelectronics, nanophotonics, microfluidics, and biotechnology, enabling the creation of cutting-edge systems and devices with improved performance. Numerous scientific and technological fields have advanced thanks to the development of photolithography, paving the door for miniaturization, integration, and innovation in various disciplines, and has become a cornerstone of modern nanofabrication.

Some of the commonly used types of photolithography include **[29]**:

- The most popular form of photolithography is optical photolithography, which transfers a pattern from a mask to a photosensitive substance deposited on a substrate using optical radiation, usually in the ultraviolet (UV) or visible spectrum. It is frequently utilized in the manufacturing of semiconductors and microelectronics.

- Extreme Ultraviolet (EUV) Lithography: Compared to optical lithography, EUV lithography produces features with finer grain sizes and higher resolution by using extreme ultraviolet light, which has a wavelength in the range of 10–14 nanometers. It is being created as a potentially effective method for cutting-edge semiconductor fabrication.

- X-ray Lithography: X-ray lithography transfers patterns onto a substrate by using X-rays with wavelengths between 0.1 and 10 nanometers. The manufacture of high-density interconnects and microelectromechanical systems (MEMS) are two examples of specific applications where it is used.

- Electron Beam Lithography: This technique uses a concentrated beam of electrons to write designs directly into a substrate. It is utilized in research labs and for specific tasks including the creation of nanostructures and gadgets because it has an incredibly high resolution.

- Nanoimprint Lithography: A photosensitive substance deposited on a substrate is imprinted with a pattern using a patterned template in nanoimprint lithography. It is a widely used method in nanofabrication because it is straightforward, affordable, and capable of achieving high resolution.

- Soft Lithography: Elastomeric stamps or templates are used in soft lithography processes like microcontact printing and microfluidic patterning to transmit patterns onto a substrate. A flexible and adaptable technique for producing microscale and nanoscale designs in a range of materials is soft lithography.

In this work, the devices were made using optical photolithography method at University of Ulsan, Department of Physics **[Fig 7]**.
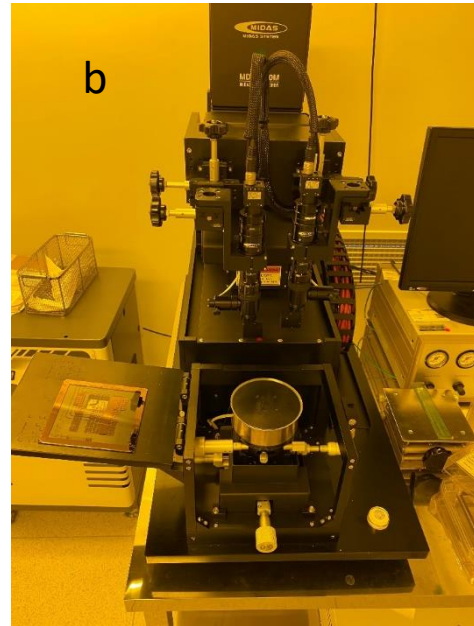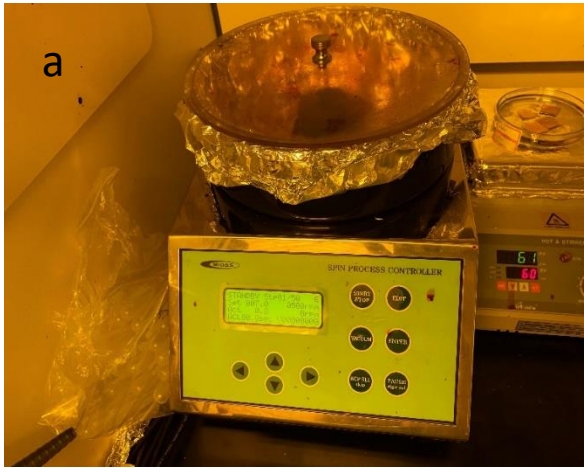
Fig 7. Photolithography system at Department of Physics, University of Ulsan, a) spin coating and b) UV photolithography

In optical photolithography, a substrate is covered with a photosensitive material, or photoresist, and a pattern is transferred onto the photoresist using a mask that has transparent and opaque areas. The photoresist undergoes a chemical or physical change when the patterned mask is in close contact to the substrate that has been covered with photoresist. The patterned areas are then revealed when the exposed photoresist is developed. These areas can subsequently be further treated via etching or other methods.

Positive photoresist and negative photoresist are the two primary categories of photoresists used in optical photolithography. Different patterns appear on the substrate as a result of these types' variations in how they react to light exposure and growth. For the scope of this work, we use the positive type named AZ GXR-601. In a positive photoresist, the unexposed portions serve as the final pattern after the development process removes the more soluble exposed regions. In other words, during development, the photoresist is removed from the exposed parts while leaving
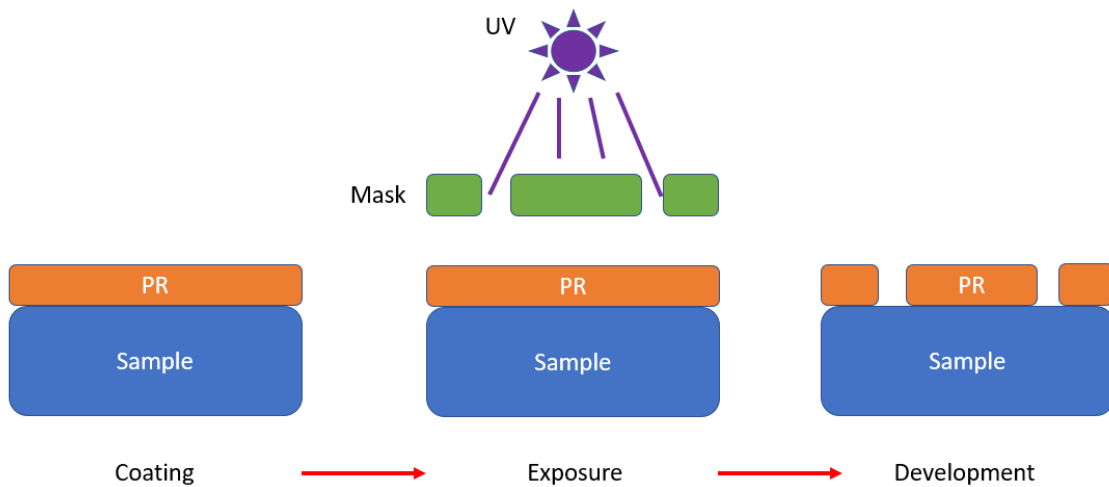
Fig 8. Positive photolithography process, PR = photoresist

the unexposed areas on the substrate. When a design with elements made of the same material as the substrate is needed, positive photoresist is frequently utilized. The process of photolithography **[Fig 8]** can be described as three steps:

1. Coating: A thin layer of positive photoresist is coated onto a substrate.

2. Exposure: A mask with a pattern of transparent and opaque regions is put close to the substrate that has been covered with photoresist. The photoresist in the exposed areas of the mask

17

undergoes a chemical change as a result of light entering through the transparent areas of the mask. The areas that are exposed become more soluble.

3. Development: The photoresist is developed, often by employing a developer solution that selectively eliminates the exposed photoresist regions, leaving the final pattern remaining in the photoresist's unexposed parts.

The result of this process is creating a firmly photoresist film with desired shape on the surface of sample. On the surface of sample, the parts covered by PR will be protected from bombarding ion milling in next step.

Fig 9. Ion milling system including a) power controller, b) cooling system and c) vacuum chamber at Department of Physics, University of Ulsan

3.3 Ion milling

After the photolithography process, the samples will now be covered with a thin film of photoresist material with desired shape. The cover parts will play important role that protecting layers of material underneath, these other parts which is revealing under the ion milling process will be decayed over time.

Ion milling is a vital technology that has become a potent tool in the creation and characterization of materials. By blasting a sample surface with ions, the precise and regulated process of "ion milling" removes material off the surface. An ion beam is used in the procedure, often focused at the sample surface and produced from an ion source like a plasma or an accelerator.

Sputtering - a popular term - is the process of atoms or molecules being expelled off the surface when ions collide with a surface and transmit their kinetic energy to the material's atoms or molecules. This causes material to be removed from the surface, resulting in surface changes.

The ion milling system used in this work is from laboratory for Spin-Orbitronic Devices, the ion milling & sputtering system, KVET-B2000, vacuum system & components, KOREA VACUUM TECH **[Fig 9]**.

3.4 X-Ray diffraction (XRD)

The X-Ray diffraction (XRD) is utilized for studying the component of thin film. When an X-ray beam passes through a crystal solid, it interacts with the lattice's electronic structure and is scattered. Since the crystal's electrons positions are periodically arranged, the scattered X-rays interfere with each other and give the information about the sample's structure. It should be noted that only when the Bragg law is satisfied, the result gives clear information about the specific positions.

$$n\lambda = 2dsin(\theta) \quad \textbf{[Eq 4]}$$

Whereas λ is the wavelength of incoming X-Ray, d is the lattice parameter and 2θ is the angle between incoming beam and scattered beam.
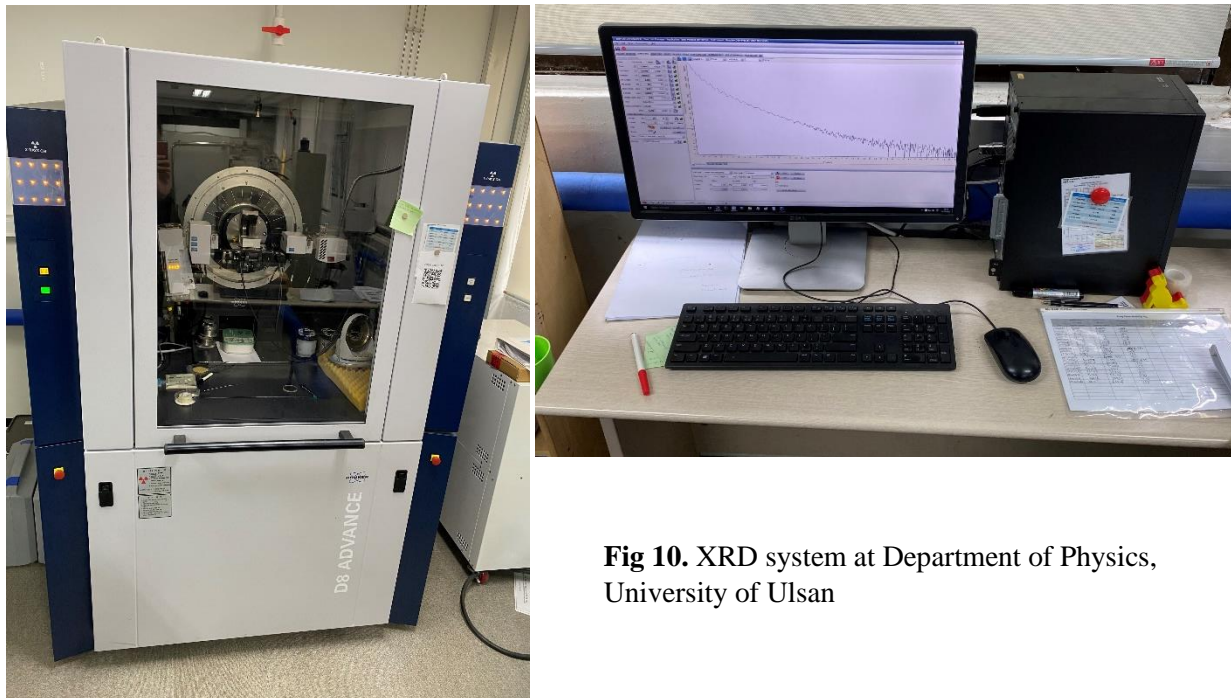
Fig 10. XRD system at Department of Physics, University of Ulsan

The XRD experiments in this work were carried on by means of a Bruker D8 Advanced diffractometer built by Bruker using Cu Kα radiation (λ ¼ 1.5406 Å) and an accelerating voltage of 40 kV and a current of 40 mA at Department of Physics, University of Ulsan **[Fig 10]**. All samples were scanned from 20° through 100° in 2θ scale with an angular step of 0.01°. The experiment schematic is presented in **[Fig 11]**. A Bragg-Brentano setup was used to perform θ - 2θ scans with the scattering vector parallel to the surface normal. In this configuration, only information about lattice planes parallel to the surface is recorded via diffraction peaks. From those positions, the lattice constant normal to the surface (out-of-plane lattice constant a_{OOP}) of the grown film can be calculated using Bragg's equation **[Eq 4]**. whereas n is the order of the corresponding reciprocal lattice vector. In heterostructures, the lattice constant of the overlying film generally does not match the lattice constant of the substrate. Deviations of the out-of-plane lattice constant a_{OOP} of the film from the bulk value might originated from the incorporation of

strain such as defect, on the other hand, unmodified a_{OOP} is achieved when the film is fully relaxed.

In addition, parasitic phases lead to additional diffraction peaks and thus can be identified in θ-2θ

scans. This allows us to determine whether the film is growing uniformly. The XRD patterns of

sample with various Cr thickness at room temperature are presented at [**Fig 12**]. It can be seen that

the MgO (200), Fe (200) and Cr (200) peak are clearly observed at $2\theta = 42,76^o$ and $64,63^o$,

respectively, which agreed well with previous work [**32, 33**].

The orientation of the grown film compared to the substrate is examined by Phi-scans

measurement. The most important step is aligning the sample and diffractometer in order to

determine a diffraction peak of the film with an in and out-of-plane component, this is mandatory
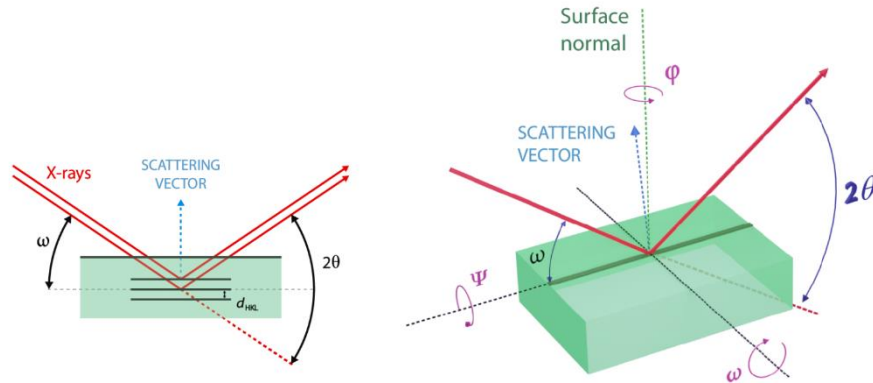
Fig 11. Experimental set up of an XRD experiment. (a) X-ray diffraction condition is satisfied only when the scattering vector matches a reciprocal space vector which is aligned perpendicular to the corresponding set of lattice planes. (b) Varied rotation angles of the sample in a four-circle X-ray diffractometer.

before carrying the experiment. After that, the sample is scanned at various angle between the

surface and incoming beam. As a result, the number of observable reflections reflects the symmetry of the film.
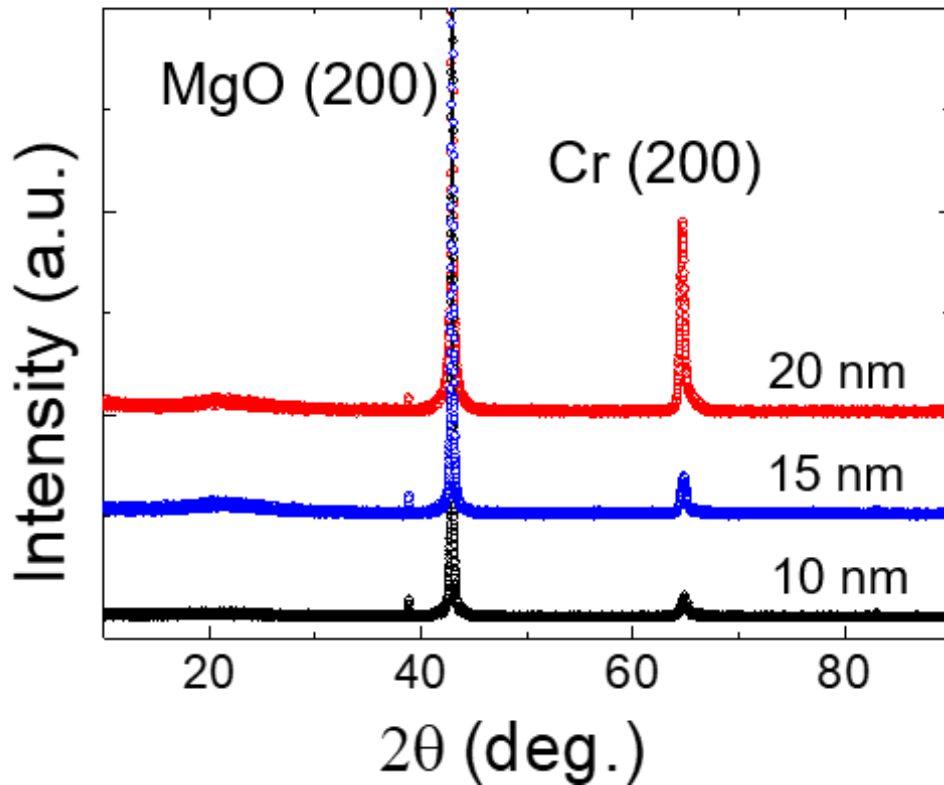
Fig 12. The XRD patterns of sample with various Cr thickness at room temperature

3.5 X-Ray reflectivity (XRR)

To measure the thickness of thin film composition, the X-Ray reflectivity is used as reliable method. The reflected X-Ray beam, which is the result of scanning $\theta - 2\theta$ incidence beam with a number of very small angles ($0^o < \theta < 3^o$), is collected. Because the reflection at the surface interferes with the reflection at the underlying interface, the measured $\theta - 2\theta$ intensity exhibits an interference fringe called the Kiessig fringe [30]. The layer thickness d can be determined from the distance $\Delta\theta$ between the intensity maxima using the relationship:

$$d = \frac{\lambda}{2 sin\Delta\theta} \qquad \textbf{[Eq 5]}$$

It should be noted that, the accuracy of the given formula is limited for thin film since the interference oscillations become very broad, in other words, thin films that are too thin might be impossible to be detected with this method. In this work, the film with thickness of Cr 20nm is expected to be observed through X-Ray reflectivity.

3.6 R_{xx} measurement

In materials science and condensed matter physics, the four-point contact method is a common method for determining a sample's electrical resistivity and Hall effect. In the study of the electrical characteristics of materials like semiconductors, metals, and insulators, where accurate measurements of resistivity and Hall coefficient are crucial, this technique is especially helpful. Four electrodes are arranged in a rectangular pattern on the sample surface using the four-point
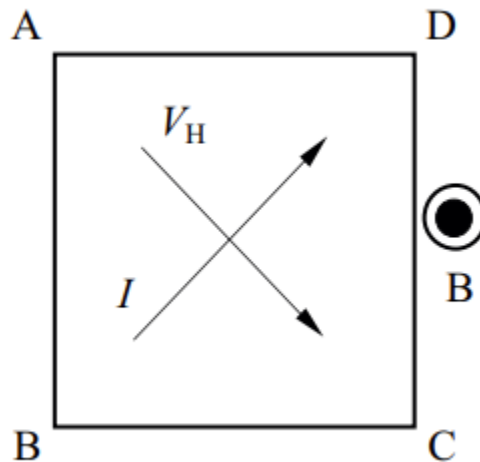
Fig 13. Four points contact for Hall measurement

contact method. Two electrodes are used to inject a current, and the remaining two electrodes are utilized to measure voltage. A current source or power supply is often used to provide the current,

and a voltmeter is used to measure the voltage. The application of a magnetic field is done perpendicular to the plane of sample, which induces a Hall voltage that can be measured to determine the Hall coefficient **[Fig 13]**.

The ability to lower contact resistance, which can have a considerable impact on the accuracy of electrical measurements in materials with high resistivity, is one of the four-point contact method's main benefits. The resistance of the contacts themselves causes contact resistance, which can cause a sizable inaccuracy in electrical measurements. The four-point contact approach minimizes the effects of contact resistance by spacing the two electrodes used to inject current from the two electrodes used to measure voltage. As a result, measurements of the sample's electrical resistivity are more precise **[31]**.

For this study, we design the device with the shape like **[Fig 14]** and set up the current I_{AB} flow from A to B, then we measure the voltage V_{CD}.
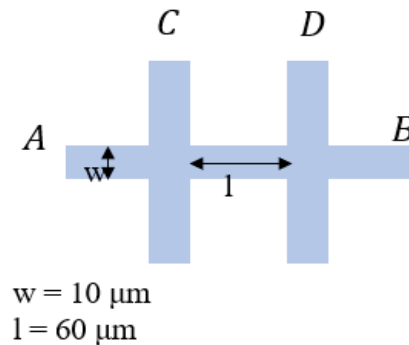

w = 10 μm
l = 60 μm

Fig 14. Device shape and the

4.   OMR at the interface of Fe/Cr bilayer

To study on the orbital Hall effect, which is the creation of a transverse spin current by an applied electric field in a material with strong spin-orbit coupling. For examining this phenomenon, the Fe/Cr bilayer system is a potential choice because it demonstrates a substantial

magnetoresistance and a significant amount of orbital hall conductivity on Cr. The orbital Hall magnetoresistance in this system is investigated using a number of experimental and analytical techniques.

The bilayer is first created using molecular beam epitaxy (MBE) at the Department of Physics, University of Ulsan. To understand the effect of substrate crystallography, we fabricate 2 sets of sample with current J_C direction **I[100]** and **I[110]** (compared to the substrate crystal direction) **[Fig 15]**. The growth condition for each layer is presented in Table 1. The thickness of Cr layer is varied at selected values: 2, 5, 7, 10, 15 and 20 nm.
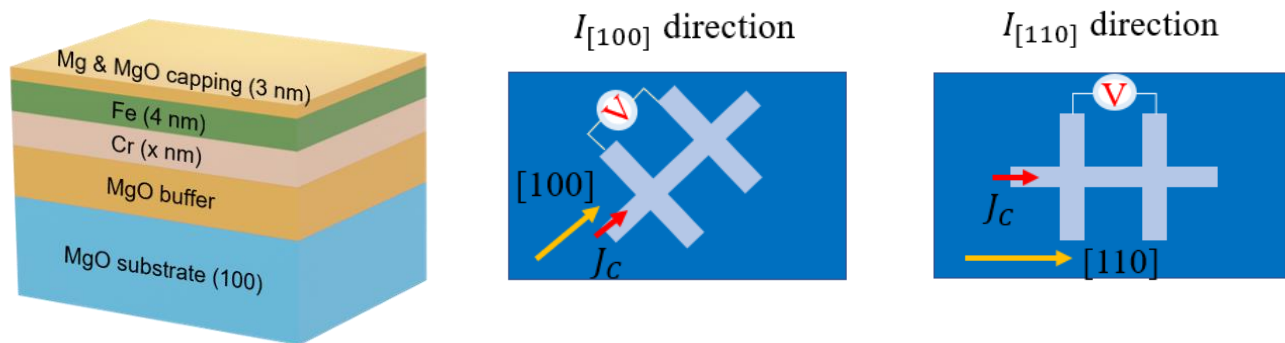
Fig 15. Sample composition and current direction
I[100] and I[110], the blue part is the substrate MgO

Layer	Growth temperature (º C)
MgO buffer	Room temperature
Cr	400
Fe	150
Mg capping	RT
MgO capping	Room temperature

Table 1. The growth condition for Fe/Cr bilayers

After the photolithography and ion milling process, the device is shaped and ready to be measured. Through the microscope images, the quality of samples is well made **[Fig 16]**.
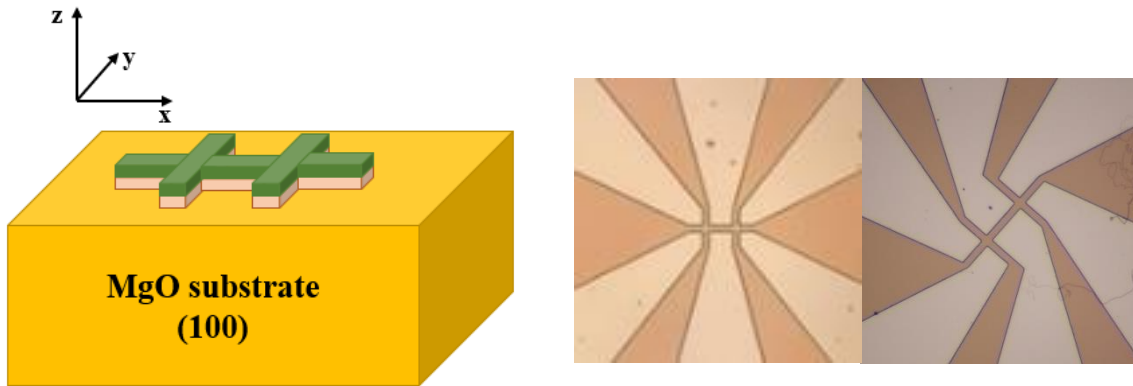
Fig 16. Sample structure and image device for I[110] and I[100] set of Fe/Cr(2nm)

The bilayer's structural and magnetic characteristics are then assessed using X-ray diffraction. X-ray diffraction and X-ray reflection provides details about the crystal structure and layer thickness. These measurements are crucial for improving the experimental setup and for comprehending how the spin current behaves in the bilayer. With a four-point probe setup, a

magnetic field of ~ 21k Oe is applied perpendicular to the direction of the current while a charge

current J_C is passed through the bilayer to measure the orbital Hall magnetoresistance **[Fig 17]**.

The amount and direction of the orbital Hall effect are then determined by analyzing the ensuing

changes in electrical resistance. Advanced mathematical simulations and models are used in this

analysis, together with careful consideration of variables like temperature and sample size. These

measurements' data can be used to derive variables like the orbital Hall angle and the orbital

diffusion length.

According to the OMR theory, the four main parameters θ_{SH}, λ_W, G_r, and P can all have an

impact on the OMR of FM/HM bilayers **[34 - 36]**. Here, θ_{SH} is the orbital Hall angle of the HM;

λ_W is the orbital diffusion length of the HM; G_r is the orbital mixing conductance at the interface

and P is the orbital polarization of the FM. It is expected that each of these characteristics is

temperature-dependent. The observed OMR values were fitted using the OMR theory as follows

[34 - 36]:

$$\frac{\Delta R_{xx}}{R_0} \sim \theta_{SH}^2 \frac{\lambda_{Cr}}{t_{Cr}} \frac{\tanh{(t_{Cr}/2\lambda_{Cr})}}{1+\xi} \left[\frac{g_R}{1+g_R\coth{(t_{Cr}/\lambda_{Cr})}} - \frac{g_F}{1+g_F\coth{(t_{Cr}/\lambda_{Cr})}} \right] \textbf{[Eq 6]}$$

$$g_R \equiv 2\rho_{Cr}\lambda_{Cr}G_r; \ g_F \equiv \frac{(1-P^2)\rho_{Cr}\lambda_{Cr}}{\rho_{Fe}\lambda_{Fe}\coth{(t_{Fe}/\lambda_{Fe})}}$$

Where R_0 is the maximum resistance of the Fe/Cr bilayer, ΔR_{xx} is difference between R_0 and

the current resistance, $t_{Fe}(t_{Cr})$ is the thickness of Fe(Cr), $\rho_{Fe}(\rho_{Cr})$ is the resistivity of the Fe(Cr)

layer, ξ represents the current shunting effect between the Cr and Fe layers and is written as:

$$\xi = \frac{\rho_{Cr}t_{Fe}}{\rho_{Fe}t_{Cr}}$$
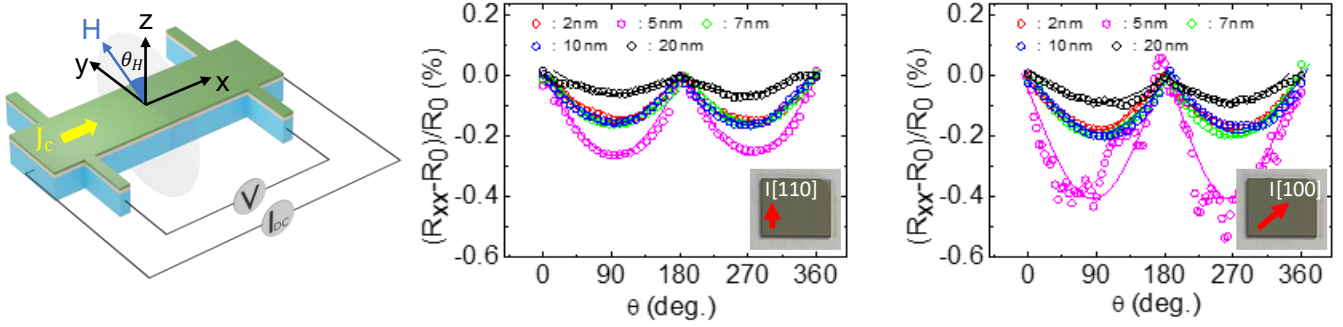
Fig 17. Angular dependent of OMR under external field 21k Oe in the yz plane

Compare to other results from previous work **[37]**, it should be noted that the upper part of resistance graph **[Fig 17]** has the sharp shape which indicates that the magnetization of FM layer has switched suddenly when the external field is perpendicular to the sample surface. The reason laying behind this phenomenon is from the saturate magnetic field of sample is higher than the field we provide (21k Oe in this work), the external field is not strong enough to make the magnetization of FM fully align with the external field **H**. In other words, there should be a different between the direction of external field **H** and the magnetization **M** of Fe. We propose a good way to calculate the missing value of that one.

For a thin film with uniaxial magnetic anisotropy where the hard axis points out of plane and all in-plane directions are equally easy, the energy E of its magnetic moment under the external magnetic field H is described as below **[38]**:

$$E = -K_1 sin^2(\theta_M) - H.M_S.cos(\theta_M - \theta_H) \text{ [Eq 7]}$$

Where the first term is magnetic anisotropy energy with the first-order constant K_1 and the second term is Zeeman energy. θ_M and θ_H are the polar angles of the magnetization M_S and the

external magnetic field **H**. When **H** $(< M_S)$ is rotating in xz and yz planes, it drags **M**, the equilibrium position of **M** should follow the below condition:

$$\frac{\partial E}{\partial \theta_M} = -2K_1 sin(\theta_M)cos(\theta_M) + H.M_S.sin(\theta_M - \theta_H) = 0$$

The relation between θ_M and θ_H can be obtained as follow:

$$\frac{2K_1}{M_S}sin(\theta_M)cos(\theta_M) = H\,sin(\theta_M - \theta_H)$$

$$\rightarrow \frac{H_K}{H} = \frac{cos(\theta_H)}{cos(\theta_M)} - \frac{sin(\theta_H)}{sin(\theta_M)} \textbf{ [Eq 8]}$$

Where $H_K = \frac{2K_1}{M_S}$ is the anisotropy field. H_K is obtained from AHE results. From **[Eq 8]** we can calculate the θ_M values corresponding to θ_H values (which data we already get in **[Fig 17]**). When **H** is at z direction, the angle between **H** and **M** is maximum $= \theta_H - \theta_M$ (hard direction) **[Fig 18]**.
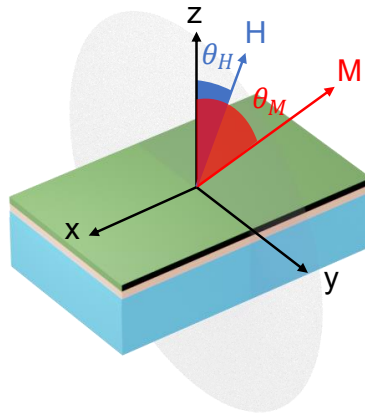
Fig 18. The relation between θ_M and θ_H

When **H** is at y direction, $\theta'_H = \theta'_M$ (easy direction)

$$\frac{H_k}{H} = \frac{\cos(\theta_H)}{\cos(\theta_M)} - \frac{\sin(\theta_H)}{\sin(\theta_M)}; \text{ when } \theta_H = 0 => \frac{H_k}{H} = \frac{1}{\cos(\theta_M)}$$

We calculate the real angle of magnetization **M** of Fe layer which is denoted as θ_M (the maximum difference between θ_M and θ_H when θ_H is parallel to z direction) **[Table 2]**

Sample	$\boldsymbol{\theta_M}(deg)$
Cr 2nm	37.1649
Cr 5nm	38.65908
Cr 7nm	39.72169
Cr 10nm	42.907783
Cr 15nm	46.98961
Cr 20nm	51.439307

Table 2. Theoretical calculation of $\boldsymbol{\theta_M}$ angle

After converting all the θ_H values to θ_M, we use a simple sin square equation to fit the real data and get the results **[Fig 19]**:
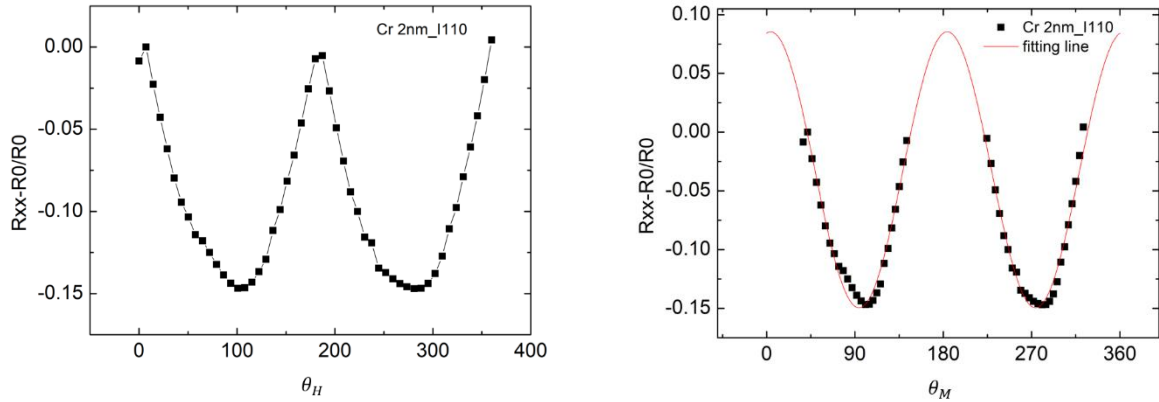

Fig 19. Converting values from θ_H to θ_M

From here, we can calculate the real OMR value from θ_M angle data **[Fig 20]**. To study the four main parameters θ_{SH}, λ_W, G_r, and P which may affect the OMR signal, we use the **[Eq 6]** and calculate the fitting line.

parameter	I[110]	I[100]
θ_{SH}	0.20192	0.24069
t_{Cr}	x	x
λ_{Cr}	$1.44781\ nm$	$1.29683\ nm$
ρ_{Cr}	$271.12634\ n\Omega.m$	$341.14581\ n\Omega.m$
G_r	$0.61 \times 10^{15}\ \Omega^{-1}m^{-2}$	$0.61 \times 10^{15}\ \Omega^{-1}m^{-2}$
P	1	1
ρ_{Fe}	$97.00035\ n\Omega.m$	$97.57827\ n\Omega.m$
λ_{Fe}	$7\ nm$	$7\ nm$
t_{Fe}	$4\ nm$	$4\ nm$

Table 3. Fitting results give value of important parameters
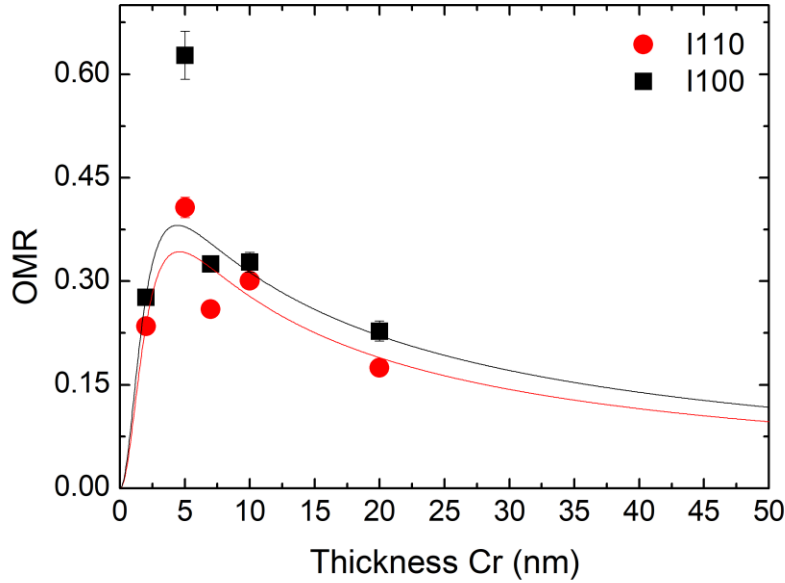
Fig 20. Thickness dependence of OMR

The fitting result shows similar trend of OMR in both case of I[110] and I[100]. The I[100] direction corresponds for larger θ_{SH} value. It should be noted that, the peak positions of the fitting results do not vary in both cases of I[100] and I[110], while the magnitudes of them are different. Since the peak position depends on the orbital diffusion length λ_{Cr}, meanwhile the amplitude corresponds to orbital Hall angle θ_{SH} and orbital mixing conductance G_r, this implies that orbital diffusion length is independence with SMR while the direction of charge current on substrate

crystal I[100] and I[110] may affect the value of orbital Hall angle. It should be noted that, although this work focuses on the OMR, there is not yet definition of orbital Hall angle, and the OMR can only indirectly interact with magnetization of FM through spin interaction, in other words, there should be orbital – spin conversion at the interface. This theory is complicate so we propose to keep the spin Hall angle for the fitting results. Further work should be carried to study about OMR and orbital Hall angle.

5. Conclusion

The study of orbital Hall magnetoresistance in Fe/Cr bilayers is an important area of research with potential applications in the field of spintronics. In this study, we investigated the orbital Hall magnetoresistance of an Fe/Cr bilayer using a four-point probe setup with two different current directions I[100] and I[110]. Our results demonstrate a clear anisotropic behavior in the magnetoresistance as a function of the orbital polarization σ of Cr and magnetization **M** of Fe, which can be attributed to the orbital Hall effect. In particular, we discovered that the magnetoresistance magnitude was substantially larger for the perpendicular ($M \perp \sigma$) arrangement than for the parallel case ($M // \sigma$). The differing contributions of the orbital current and the orbital accumulation effect can be used to explain this discovery, which is in line with earlier research on orbital Hall magnetoresistance in other systems **[37]**.

Furthermore, we observed a clear dependence of the magnetoresistance on the thickness of the Cr layer, with a maximum effect occurring at an Cr thickness of around 5 nm. This behavior can be explained by the interplay between the orbital Hall effect and the magnetic properties of the Cr layer, which depend strongly on the thickness.

Theoretical simulations based on the orbital-diffusion equation have provided further insight into the physics of orbital Hall magnetoresistance in Fe/Cr bilayers. These simulations confirmed the existence of lateral orbital currents in the bilayer and allowed us to extract parameters such as orbital Hall angle and orbital diffusion length.

In this work, we also fabricate 2 sets of difference of charge current direction with expectation that the OMR result in 2 cases will be different, however, the trend in both cases is similar which

indicates that the OMR in Fe/Cr layer on MgO substrate of I[100] larger than I[110] which indicates the OMR in Fe/Cr layer is independence on the charge current on substrate direction.

In summary, our work provides important new insights into the behavior of orbital-Hall magnetoresistance in Fe/Cr bilayers, and the dependence of current direction and Cr thickness in determining the magnitude and anisotropy of the effect. These results have important implications for the design and optimization of spintronic devices based on Fe/Cr bilayers and may point the way for future research in this exciting field. The fabrication method including photolithography and ion milling as well as the quality observation of XRD are also mentioned in this work.

References

1. Dyakonov M I 2007 Phys. Rev. Lett. 99 126601

2. Weiler, M.; Althammer, M.; Czeschka, F. D.; Huebl, H.; Wagner, M. S.; Opel, M.; Imort, I.-M.; Reiss, G.; Thomas, A.; Gross, R.Local Charge and Spin Currents in Magnetothermal Landscapes. Phys. Rev. Lett. 2012, 108, 106602

3. M. I. Dyakonov and V. I. Perel (1971). "Possibility of orientating electron spins with current". Sov. Phys. JETP Lett. 13: 467.

4. M. I. Dyakonov & V. I. Perel (1971). "Current-induced spin orientation of electrons in semiconductors". Phys. Lett. A. 35

5. Tanaka, T. et al. Intrinsic spin Hall effect and orbital Hall effect in 4d and 5d transition metals. Phys. Rev. B 77, 165117 (2008).

6. Kontani, H., Tanaka, T., Hirashima, D. S., Yamada, K. & Inoue, J. Giant orbital Hall effect in transition metals: origin of large spin and anomalous Hall effects. Phys. Rev. Lett. 102, 016601 (2009)

7. Go, D., Jo, D., Kim, C. & Lee, H.-W. Intrinsic spin and orbital Hall effects from orbital texture. Phys. Rev. Lett. 121, 086602 (2018).

8. Jo, D., Go, D. & Lee, H.-W. Gigantic intrinsic orbital Hall effects in weakly spin-orbit coupled metals. Phys. Rev. B 98, 214405 (2018)

9. Ding, S. et al. Harnessing orbital-to-spin conversion of interfacial orbital currents for efficient spin-orbit torques. Phys. Rev. Lett. 125, 177201 (2020).

10. Bader S D and Parkin S S P 2010 Annu. Rev. Condens. Matter Phys. 1 71

11. Sinova J and Žutić I 2012 Nat. Mater. 11 368

12. Thomson W 1857 Proc. R. Soc. Lond. 8 546

13. McGuire T R and Potter R I 1975 IEEE Trans. Magn. MAG-11 1018

14. Thompson D A, Romankiw L T and Mayadas A F 1975 IEEE Trans. Magn. **MAG-11** 1039

15. Pippard, A.B. (1989). Magnetoresistance in Metals. Cambridge University Press. ISBN 978-0-521-32660-5

16. Fert A 2008 Rev. Mod. Phys. 80 1517

17. Yuasa S 2008 J. Phys. Soc. Japan 77 031001

18. Moodera J S, Miao G-X and Santos T S 2010 Phys. Today 63 46

19. M. Z. Hasan and C. L. Kane, Rev. Mod. Phys. 82, 3045 (2010).

20. S. R. Park, C. H. Kim, J. Yu, J. H. Han, and C. Kim, Phys. Rev. Lett. 107, 156803 (2011).

21. D. Go, J.-P. Hanke, P. M. Buhl, F. Freimuth, G. Bihlmayer, H.-W. Lee, Y. Mokrousov, and S. Blügel, Sci. Rep. 7, 46742 (2017).

22. V. Sunko, H. Rosner, P. Kushwaha, S. Khim, F. Mazzola, L. Bawden, O. J. Clark, J. M. Riley, D. Kasinathan, M. W. Haverkort, T. K. Kim, M. Hoesch, J. Fujii, I. Vobornik, A. P. Mackenzie, and P. D. C. King, Nature (London) 549, 492 (2017).

23. J.-H. Park, C. H. Kim, H.-W. Lee, and J. H. Han, Phys. Rev. B 87, 041301 (2013).

24. M. Ünzelmann, H. Bentmann, P. Eck, T. Kißlinger, B. Geldiyev, J. Rieger, S. Moser, R. C. Vidal, K. Kißner, L. Hammer, M. A. Schneider, T. Fauster, G. Sangiovanni, D. Di Sante, and F. Reinert, Phys. Rev. Lett. 124, 176401 (2020).

25. D. Go, D. Jo, T. Gao, K. Ando, S. Blügel, H.-W. Lee, and Y. Mokrousov, Phys. Rev. B 103, L121113 (2021).

26. H. Nakayama, M. Althammer, Y.-T. Chen, K. Uchida, Y. Kajiwara, D. Kikuchi, T. Ohtani, S. Geprägs, M. Opel, S. Takahashi, R. Gross, G. E. W. Bauer, S. T. B. Goennenwein, and E. Saitoh, Phys. Rev. Lett. 110, 206601 (2013).

27. J. Sinova, S. O. Valenzuela, J. Wunderlich, C. H. Back, and T. Jungwirth, Rev. Mod. Phys. 87, 1213 (2015).

28. M. D. Stiles and A. Zangwill, Phys. Rev. B 66, 014407 (2002)

29. Sreenivasan, S. V. (2013). Introduction to Nanotechnology and Photolithography. CRC Press.

30. H. Kiessig, "Interferenz von Röntgenstrahlen an dünnen Schichten", Annalen der Physik 402, 769, (1931) doi:10.1002/andp.19314020702 (cited on page 18).

31. Kinder, Rudolf, Mikolášek, Miroslav, Donoval, Daniel, Kováč, Jaroslav and Tlaczala, Marek. "Measurement Systemwith Hall and a Four Point Probes for Characterization of Semiconductors" Journal of Electrical Engineering, vol.64, no.2, 2013, pp.106-111. https://doi.org/10.2478/jeec-2012-0015.

32. Fermin, Jose. (2016). Surface Magneto-Optical Kerr Effect Study of Magnetization Reversal in Epitaxial Fe(100) Thin Films. Research & Reviews: Journal of Material Sciences. 04. 10.4172/2321-6212.1000134

33. Elsukov, Evgeny & Kolodkin, Denis & Ul'yanov, Alexander & Porsev, Vitaly. (2014). Probe Mössbauer spectroscopy of mechanical alloying in binary Cr-57Fe (1 at%) system. AIP Conference Proceedings. 1622. 114-119. 10.1063/1.4898619.

34. J. Kim, P. Sheng, S. Takahashi, S. Mitani, and M. Hayashi, Phys. Rev. Lett. 116, 097201 (2016)

35. J. Liu, T. Ohkubo, S. Mitani, K. Hono, and M. Hayashi, Appl. Phys. Lett. 107, 232408 (2015).

36. Y.-T. Chen, S. Takahashi, H. Nakayama, M. Althammer, S. T. B. Goennenwein, E. Saitoh, and G. E. W. Bauer, Phys. Rev. B 87, 144411 (2013).

37. Takaya Okuno et al 2016 Jpn. J. Appl. Phys. 55 080308

38. Tang, M., Huang, J., Qin, F. et al. Continuous manipulation of magnetic anisotropy in a van der Waals ferromagnet via electrical gating. Nat Electron 6, 28–36 (2023). https://doi.org/10.1038/s41928-022-00882-z